PERGAMON

Vision Research 40 (2000) 3145–3157

Vision Research

www.elsevier.com/locate/visres

Calculating the contrasts that retinal ganglion cells and LGN neurones encounter in natural scenes

Y. Tadmor [a,*], D.J. Tolhurst [b]

[a] *Department of Psychology, University of Newcastle, Newcastle upon Tyne, NE1 7RU, UK*
[b] *The Department of Physiology, University of Cambridge, Downing Street, Cambridge, CB2 3EG, UK*

Received 23 February 1998; received in revised form 22 April 2000

Abstract

Visual responses are known to depend on stimulus contrast and not simply on the absolute levels of retinal illumination. Here, we have determined the contrasts that mammalian retinal ganglion cells and lateral geniculate neurones (LGN) are likely to encounter in real world scenes. Local contrasts were calculated in 135 calibrated images of a variety of real world scenes using contrast operators that closely mirror the characteristic receptive-field organisation of mammalian retinal ganglion cells and LGN neurones. We have found that the frequency distribution of the calculated local contrasts has a pronounced peak at zero contrast and that it tails off roughly exponentially with increasing positive and negative contrasts; about 90% of the contrasts in the images were within the equivalent range of ± 0.5 Michelson and Weber contrasts. Further analysis suggests that the characteristic forms of the contrast-response functions of mammalian retinal and LGN neurones are matched to the range of contrasts that they experience when viewing real world images.

Keywords: Local contrast; Natural images; Difference-of-Gaussians; Retinal ganglion cells; LGN neurones

1. Introduction

The responses of mammalian retinal ganglion cells and of neurones in the lateral geniculate nucleus (LGN) do not depend only on the absolute levels of retinal illumination (I); nor do they depend simply on the difference in the illumination (ΔI) of their antagonistic receptive field regions. Rather, over a large range of background intensities ($\bar{I}$), these neurones adapt to light in a manner that makes their responses depend on stimulus contrast: $\Delta I/\bar{I}$ (Barlow, 1969a; Barlow & Levick, 1969a,b; Jacobs, 1969; Sakmann & Creutzfeldt, 1969; Shapley & Enroth-Cugell, 1984; Purpura, Kaplan, & Shapley, 1988; Troy & Enroth-Cugell, 1993).

This neural transformation of luminance signals into contrast is thought to serve two interrelated goals. First, it scales down the vast range of ambient illuminations into signals that, otherwise, could not be accommodated within the limited dynamic response ranges of visual neurones. Secondly, contrast signals enable the visual system to represent the reflectance of objects (von Helmholtz, 1924; Laughlin, 1983; Shapley & Enroth-Cugell, 1984) so that the neurones' responses to real-world objects are unaffected by changes in ambient illumination. Indeed, daily variations of ambient illumination may span a range of about ten orders of magnitude (Martin, 1983) while the reflectances of natural objects vary only over a much smaller range, from about 5 to about 85% (Wyszecki & Stiles, 1982).

But how suitable are the limited dynamic response ranges of visual neurones for encoding the range of contrasts found in the natural environment? This question was addressed explicitly by Laughlin (1981) who measured the responses of fly retinal second-order neurones (LMC) as a function of the Weber contrast of a spot of light presented on a background; he compared the resulting contrast-response functions with the range of contrasts he calculated from one-dimensional luminance scans of natural scenes. Laughlin found that the sigmoidal form of the fly contrast-response function follows closely the form of the cumulative probability distribution of contrasts in natural scenes; thus, these neurones encode the contrasts in their natural environment efficiently.

* Corresponding author. Tel.: +44-191-2226263.
E-mail address: yoav.tadmor@ncl.ac.uk (Y. Tadmor).

0042-6989/00/$ - see front matter
PII: S0042-6989(00)00166-8

It is important to recognise that, while the contrast of a spot of light is readily specified by the Weber definition of contrast, there is no such unique definition for the contrast of a real-world scene (Peli, 1990; Tadmor & Tolhurst, 1994; Tolhurst & Tadmor, 1997) or even that of a Gabor patch (Peli, 1997). Thus, to transform the luminance scans of natural scenes into contrast, Laughlin had to choose an appropriate 'contrast operator', *one whose spatial characteristics closely mirrored the receptive field he was studying*. In essence, his contrast operator was a computational model of the receptive-field of the fly LMC neurone. Laughlin was able to compare the contrast distribution in natural scenes directly with the responses of the fly neurones to spots of light because his contrast operator evaluated contrast in an equivalent way to the Weber definition of contrast (Eq. (10)).

In this paper, we examine whether *mammalian* retinal ganglion cells and LGN neurones are also suited for encoding the contrast in natural scenes efficiently. Since the receptive-field dimensions of these mammalian neurones differ markedly from those of fly LMC neurones, we must evaluate contrast in natural scenes using a different contrast operator from the one used in the fly, one that mirrors the receptive-field organisation of mammalian neurones. Only then can we examine whether the characteristic forms of mammalian contrast-response functions suit them for coding the contrast information that *they* encounter in natural scenes. Some of this work has been reported briefly (Tadmor & Tolhurst, 1995)

2. Models and procedures

2.1. Contrast operators

Our analysis of the contrasts in natural scenes was done with contrast operators that were based on the difference of Gaussians (DOG) receptive-field model (Rodieck, 1965; Enroth-Cugell & Robson, 1966). The DOG model has been used successfully in many studies to describe the receptive fields and responses of mammalian retinal ganglion cells and LGN neurones. However, as we describe below, we have had to modify the DOG model to produce an output that depends on stimulus contrast and not simply on local luminance differences alone.

2.1.1. The conventional DOG model

In the conventional model, the spatial sensitivity of the receptive-field centre alone is described by a 2-dimensional, circularly-symmetric Gaussian with a peak amplitude of 1.0:

$$\text{Centre}(x,y) = \exp[-(x/r_c)^2 - (y/r_c)^2] \quad (1)$$

where, r_c, or the 'radius' of the centre, represents the distance over which sensitivity falls to 1/e of the peak value. The surround component of the receptive field is described by a second Gaussian, with a larger radius, r_s; in our implementation of the DOG model, we use:

$$\text{Surround}(x,y) = 0.85\,(r_c/r_s)^2 \exp[-(x/r_s)^2 - (y/r_s)^2] \quad (2)$$

where the scaling factor of $0.85 \cdot (r_c/r_s)^2$ sets the integrated sensitivity (or volume) of the surround component to be 85% of that of the centre. This scaling factor is representative of the values reported for retinal ganglion cells and LGN neurones of cat and monkey (e.g. Enroth-Cugell & Robson, 1966; Linsenmeier, Frishman, Jakiela, & Enroth-Cugell, 1982; Derrington & Lennie, 1982, 1984; Irvin, Casagrande, & Norton, 1993; Croner & Kaplan, 1995; Donner & Hemilä, 1996; Benardete & Kaplan, 1997a). Note that the final conclusions of our analysis are not affected by this particular choice of 85%.

When the midpoint of a receptive-field centre is at spatial co-ordinates $[x,y]$ of a stimulus image, the output of the centre component is:

$$R_c(x,y) = \sum_{i=x-3r_c}^{x+3r_c} \sum_{j=y-3r_c}^{y+3r_c} \text{Centre}(i-x, j-y) \cdot \text{Picture}(i,j) \quad (3)$$

where the distance of $3r_c$ from the receptive-field midpoint ensures that the sensitivity of the centre has fallen virtually to zero. The variable Picture represents a sinusoidal luminance grating, a spot of light or a natural scene, as we describe below.

The output of the receptive-field surround component is calculated in a similar way:

$$R_s(x,y) = \sum_{i=x-3r_s}^{x+3r_s} \sum_{j=y-3r_s}^{y+3r_s} \text{Surround}(i-x, j-y) \cdot \text{Picture}(i,j) \quad (4)$$

The conventional DOG model (Rodieck, 1965; Enroth-Cugell & Robson, 1966), describes the response of a retinal ganglion cell or an LGN neurone as a subtraction of Eq. (4) from Eq. (3) (the surround output from the centre output):

$$\text{DOG model response}(x,y) = R_c(x,y) - R_s(x,y) \quad (5)$$

Thus, the conventional DOG model postulates that the response of a neurone depends only on local luminance differences (ΔI) between the receptive-field centre and surround. However, it is known that, owing to the process of light adaptation, the response gain of retinal ganglion cells and LGN neurones is set by the local mean luminance ($\bar{I}$) in a manner that makes their responses depend on stimulus contrast, $\Delta I/\bar{I}$ (Shapley & Enroth-Cugell, 1984). *Thus, the DOG model must be modified to include a normalising division by the local*

mean luminance ($\bar{I}$) in order to make the model's output dependent on contrast. This modification is particularly important in our case since we wish to determine the local contrasts in real-world images, where local mean luminance changes significantly from one image location to another. In our sample of 135 real-world images (see below) the local mean luminance (averaged over 32×32 pixels) ranged by a factor of 4–40 within individual images and by a further factor of 3 between images (i.e. a total range of 120 times).

Unfortunately, the physiological information necessary to modify the DOG model accurately is, as yet, unavailable. In particular, we do not yet know the size of the adaptation pool (Rushton, 1965), i.e. the retinal region over which the local mean luminance is evaluated by a neurone. Some studies have found that the adaptation pool is of the same size as the receptive-field centre, while others have found that it is as big as the surround (see Section 4).

2.1.2. A modified DOG model

In the absence of conclusive physiological guidance we have decided to examine three hypothetical schemes of the spatial organisation of the adaptation pool. In the first scheme, *the centre-only adaptation scheme*, the mean luminance is assumed to be a weighted evaluation over the same retinal area as the centre component of the receptive-field, as has been suggested in the cat (Cleland & Enroth-Cugell, 1968; Enroth-Cugell, Lennie, & Shapley, 1975; Shapley & Enroth-Cugell, 1984). More specifically, we assume that the divisive effect of light adaptation is a function of the output of the receptive-field's centre component:

$$\text{Contrast output}(x,y) = \frac{R_c(x,y) - R_s(x,y)}{R_c(x,y)} \tag{6}$$

In macaque P ganglion-cells, however, the gain of the neurone can be influenced by steady lights falling in the receptive-field surround (Kaplan & Shapley, 1989; Benardete & Kaplan, 1997b) or even beyond (Valberg, Lee, & Tigwell, 1985). Thus, in our second scheme, *the surround-only adaptation scheme*, the divisive effect of light adaptation is assumed to be a function only of the output of the surround component of the receptive field:

$$\text{Contrast output}(x,y) = \frac{R_c(x,y) - R_s(x,y)}{R_s(x,y)} \tag{7}$$

Our third scheme is a hybrid, in which the adaptation pool is considered to be of the same size as the receptive-field surround but is more heavily weighted in favour of the field centre than it is in Eq. (7). Thus, the divisive effect of light adaptation is a function of the outputs of *both* the centre and the surround components of the receptive field:

$$\text{Contrast output}(x,y) = \frac{R_c(x,y) - R_s(x,y)}{R_c(x,y) + R_s(x,y)} \tag{8}$$

Note the similarity between Eq. (7) and the Weber definition of stimulus contrast (Eq. (10) below), and between Eq. (8) and the Michelson definition of grating contrast (Eq. (9) below).

2.2. Calculating contrast

Such models of spatial summation and light adaptation could be used to calculate the response of a neurone to any arbitrary stimulus, provided that they also incorporate the compressive non-linear relationship between the rate of generation of action potentials and stimulus magnitude. However, by ignoring that compressive response non-linearity, in the first instance, the output of the above 'model receptive-fields' can be used to provide a measure of the local contrast, as seen by the neurones. The receptive-fields are *contrast operators* rather than complete models of real neurones. In Section 4, we will explicitly examine the significance of the compressive non-linearity for the coding of contrast.

We have used 24 different receptive-field models as contrast operators, with the following spatial characteristics: three different receptive-field centre sizes (r_c) of 2.0, 3.0 and 4.0 pixels (see below for actual sizes) and, for each centre size, eight different ratios of surround-to-centre size (r_s/r_c) ranging from 2.0 to 9.0. This range of the spatial parameters is representative of that reported for retinal ganglion cells and LGN neurones in the cat and the monkey (e.g. Enroth-Cugell & Robson, 1966; Linsenmeier et al., 1982; Derrington & Lennie, 1982, 1984; Irvin et al., 1993; Croner & Kaplan, 1995; Benardete & Kaplan, 1997a).

For each of these 24 contrast operators, we have first calculated the spatial frequency and phase of a sinusoidal grating and the diameter of a spot of light that gave the largest output. The spatial frequency of the optimal grating and the diameter of the optimal spot depended obviously on r_c and r_s, but they were also affected slightly by the particular light-adaptation scheme used. We have, therefore, determined the optimal stimuli for each operator and for each of the light adaptation schemes separately.

These spatially-optimal stimuli were then used to determine the dependence of an operator's output on the contrast of sinusoidal luminance gratings and of spots of light. The contrasts of the sinusoidal luminance gratings were specified by the conventional Michelson definition:

$$\text{Michelson contrast} = \frac{L_{max} - L_{min}}{L_{max} + L_{min}} \text{ or } \frac{L_{max} - L_{mean}}{L_{mean}} \tag{9}$$

where L_{max} and L_{min} are the maximal and minimal luminances of the grating. Michelson contrast was defined as 'positive' when a bright bar of the grating was superimposed on the centre of an 'ON'-centre contrast operator and as 'negative' when a dark bar of the grating was centred on the operator (i.e. a 180° shift of the spatial phase). An 'OFF'-centre contrast operator would be modelled simply by negating the numerators in Eqs. (6)–(8). Thus, in the following analyses, negative outputs can be considered as the positive outputs of OFF-centre contrast operators.

The contrasts of the spots of light were specified by the conventional Weber definition:

$$\text{Weber contrast} = \frac{L_{spot} - L_{background}}{L_{background}} \quad (10)$$

Similarly, positive Weber contrasts correspond to a spot of light centred on the receptive field and of a luminance higher than that of the background, while negative Weber contrasts correspond to the case where the spot was dimmer than the background. Note that, in Eqs. (9) and (10), the divisors both tend to become simple measures of the space-averaged mean luminance of the *whole* stimulus when the period of the grating or the diameter of the spot of light are small compared to the size of the whole stimulus.

We have also used Eqs. (6)–(8) to calculate the outputs of each contrast operator in response to images of natural scenes. The analysis was done on an ensemble of 135 real-world images representing a variety of objects and scenes (e.g. landscapes, plants, animals, people, faces, buildings). The photographs were digitised and calibrated as described by Tolhurst, Tadmor, and Tang Chao (1992). Briefly, the images were digitised from negatives to a spatial resolution of 256×256 pixels and to a nominal luminance resolution of about 1000 grey levels. The photographs were taken with a camera having a 50 mm lens and an aperture of F8. The 35 mm negatives covered a field of view of about 25×35 deg, and a square segment of the negative, measuring about 25×25 deg, was digitised to a resolution of 256×256 pixels. Each pixel thus represents approximately 6×6 min. It should be noted, however, that this absolute scale is not particularly meaningful, since we could have taken exactly the same photographs in many cases with lenses of different magnification (or field of view) while adjusting our viewing distance appropriately. Furthermore, Fig. 4A will show that absolute scale is relatively unimportant to our analyses.

Each film-roll also included negatives of Munsell grey-paper charts whose luminance we measured. These were developed and digitised along with the photographs of the natural scenes. We used these reference grey-level charts to convert each pixel value in a digitised image into its actual luminance value, and thereby corrected for the luminance non-linearities of the film.

The complete analysis was done for each of the 24 contrast operators at 1000 randomly-chosen positions within each of the 135 images of natural scenes (i.e. a total of over 3.2 million samples). The random positions were constrained so that the mid-point of any model receptive-field was always at least $3r_s$ pixels from the margins of the photograph in order to eliminate spurious edge-effects.

3. Results

3.1. The contrasts in a natural scene

Fig. 1 shows the range of outputs obtained by applying one contrast operator to the image of the tree branches, shown as the inset to Fig. 1C. The contrast operator had a surround:centre radius ratio (r_s/r_c) of 2.0 and a centre size (r_c) of 2.0 pixels; the image measured 256×256 pixels. We have calculated the outputs of this operator at 1000 randomly-chosen positions within the image (see Section 2) and the three histograms (A, B & C) show the frequency of different output levels for each of the three light-adaptation schemes: centre-only scheme (Eq. (6), Fig. 1A), surround-only scheme (Eq. (7), Fig. 1B) and centre-plus-surround scheme (Eq. (8), Fig. 1C).

Clearly, the three histograms are not identical, even though the contrast operator was applied at the same 1000 locations in the photograph. The histograms agree neither on the range nor on the exact form of the distribution of calculated contrasts in the image. Since the three light-adaptation schemes produce different answers, it is *not* immediately possible to infer the local contrasts in this real world scene from the outputs of the contrast operator. In his analysis of the contrasts in real world scenes, Laughlin (1981) used the one-dimensional analogue of the light adaptation scheme in Fig. 1B: the surround-only adaptation scheme, which mirrors the Weber definition of contrast (Eq. (10)).

In order to understand why the different light-adaptation schemes produce such different distributions of contrasts in the natural image, we have applied this contrast operator to a geometrically-simple stimulus of well-defined contrast: a sinusoidal luminance grating of different Michelson contrasts whose spatial frequency and spatial phase were optimal for the spatial characteristics of this operator (see Section 2).

Fig. 2 shows the calculated output of the same contrast operator as in Fig. 1 as a function of the Michelson contrast of a sinusoidal luminance grating. Positive values on the contrast axis represent the case where a bright bar of the grating is centred on the receptive-field's ON-centre, whereas negative values on the contrast axis represent the case where a dark bar is centred on the ON-centre (a 180° phase shift of the

grating). The three graphs show the calculated output for the three light-adaptation schemes: centre-only scheme (●), surround-only scheme (○) and the centre-plus-surround scheme (△).

It can be seen that the three graphs have different dependencies on the grating's contrast and that none of them is a straight line. Furthermore, the outputs of the operator to positive and negative contrasts are not mirror-images of each other. The dependency of the surround-only scheme (○) on stimulus contrast is the nearest to a straight line, while that for the centre-only scheme (●) is the most curved. We have repeated this contrast analysis using contrast operators with different surround:centre ratios (i.e. different r_s/r_c values) and have found similar non-linear dependencies on the contrast of gratings, with the exception that the contrast-output functions of the surround-only adaptation scheme (○) become increasingly more linear as r_s/r_c is made larger. Such a trend can be explained in the following way: as r_s gets larger, the surround mechanism alone provides an increasingly better measure of the mean luminance of the *whole* stimulus and, thus, the surround-only adaptation scheme becomes increasingly more similar to the actual definition of stimulus contrast (Eq. (9)), in which mean luminance is defined over the *whole* spatial extent of the stimulus.

We have repeated this contrast analysis with spatially-optimal spots of light of different Weber contrasts (Eq. (10)) instead of the sinusoidal luminance gratings, with almost identical results. Again, we have found that the contrast-output functions are not directly proportional to the Weber contrast of the spot stimuli, except for the surround-only adaptation scheme in models with large surround:centre ratios. Only in such cases does the output of a contrast operator provide a *direct* measure of stimulus contrast. It is significant, therefore, that Laughlin's (1981) model neurone for the fly had a particularly large surround:centre ratio.

Although the three light-adaptation schemes in Fig. 2 seem to provide different measures of stimulus contrast, it can also be seen that, within a given light-adaptation scheme, there are qualitative similarities between the outputs to the natural image (Fig. 1, abscissa) and the outputs to the sinusoidal luminance grating (Fig. 2, ordinate). For instance, the centre-only adaptation scheme in Fig. 1A shows a long tail of negative values and very few positive ones above a value of $+0.4$; the same scheme (●) in Fig. 2 produces large negative

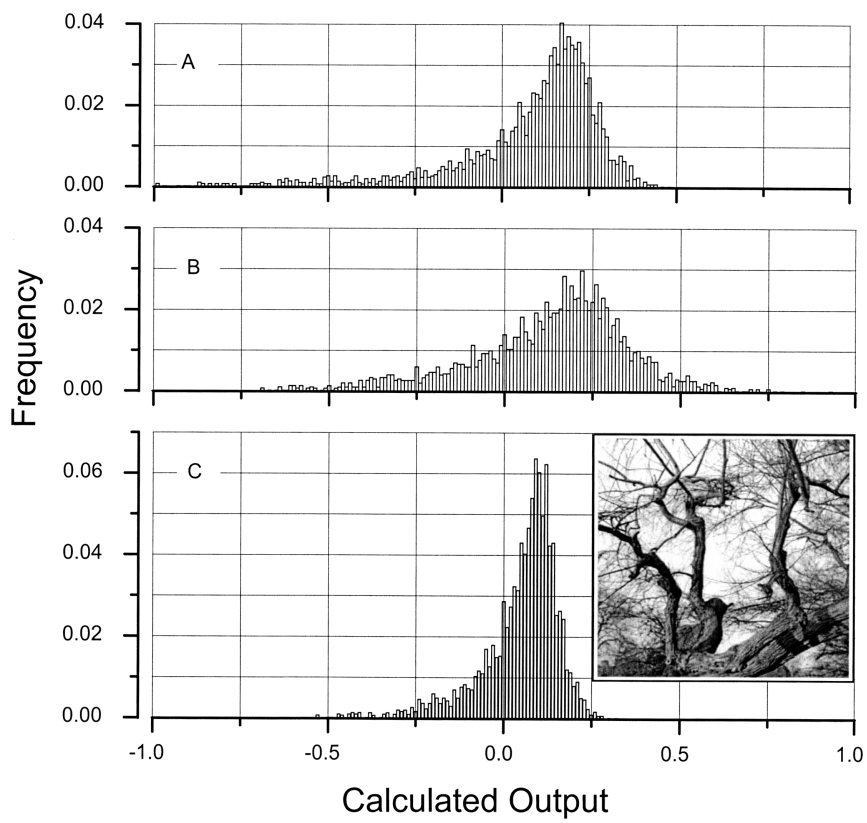

Fig. 1. The distribution of the output of a contrast operator calculated at 1000 locations within a digitised photograph of the branches of a tree (shown inset in panel C). The operator had a centre radius (r_c) of 2.0 pixels, and a surround:centre ratio (r_s/r_c) of 2.0. The photograph measured 256×256 pixels. The behaviour is shown for three different light-adaptation schemes: the centre-only (A), the surround-only (B) and the centre-plus-surround (C). The histograms show the frequency (out of 1000 stimulation points) of obtaining each particular output value. The calculated output is in arbitrary units.

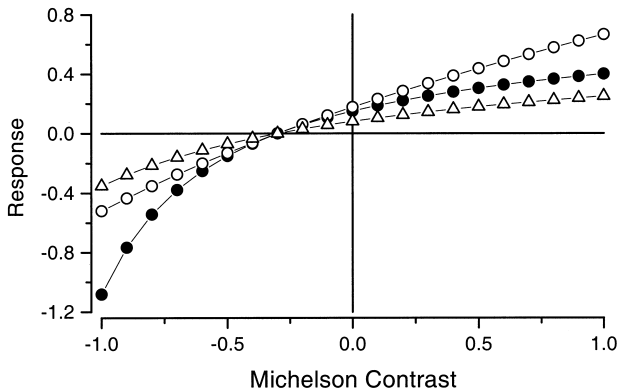

Fig. 2. The dependence of calculated output on the Michelson contrast of a sinusoidal luminance grating of optimal spatial frequency is shown for the same contrast operator as in Fig. 1, i.e. with centre radius (r_c) of 2.0 pixels, and a surround:centre ratio (r_s/r_c) of 2.0. The gratings measured 256×256 pixels and contrast was specified by the Michelson definition (Eq. (9)). The calculated output is in the same arbitrary units as in Fig. 1. The three graphs show the results for the three different light-adaptation schemes: the centre-only (●), the surround-only (○) and the centre-plus-surround (△). The sinusoidal gratings were optimally positioned and had the optimal spatial frequency determined separately for each adaptation scheme. Note that in all three graphs zero contrast does not elicit zero output. This is because the responsivity of the surround component of the receptive field was set to be 85% of that of the centre mechanism (Eq. (2)) and, therefore, there is incomplete cancellation of the centre response (R_c) to the average luminance. The centre-plus-surround scheme (△) produces the smallest outputs because the divisor is larger than in the other two schemes.

values while positive ones do not exceed $+0.4$. The surround-only adaptation scheme in Fig. 1B shows frequent values up to about 0.7 in agreement with Fig. 2 (○) where the maximum value is about 0.7. The centre-plus-surround adaptation scheme has the lowest outputs both to the grating (△ in Fig. 2) and to the natural scene (Fig. 1C). Lastly, it can be seen that the modes of the three histograms in Fig. 1 are at similar output values as those of the corresponding light adaptation schemes to zero Michelson contrast in Fig. 2.

3.1.1. Equivalent contrast

These qualitative similarities between the calculated outputs of the contrast operator to gratings and to the image led us to test whether the differences in the form of the three histograms in Fig. 1 can, in fact, be explained completely by the differences in the forms of the three contrast-output functions in Fig. 2. We have done this by using the appropriate contrast-output function of each light-adaptation scheme in Fig. 2 as a 'look-up' table which maps each calculated output to the natural image into an *equivalent Michelson contrast*: the Michelson contrast of the optimal sinusoidal luminance grating that elicited an identical output to that calculated in the digitised photograph. The transformation was done for each light-adaptation scheme separately and the results are shown as the three histograms in Fig. 3.

It can be seen that the three new distributions are so similar to each other as to be almost indistinguishable. Thus, the initial differences in the forms of the output histograms for the three light adaptation schemes when stimulated by a natural image (Fig. 1) are completely accounted for by differences in their outputs to simple stimuli (Fig. 2); the distribution of the equivalent Michelson contrasts in a natural image is independent of the particular light-adaptation scheme used. An identical result is obtained when the responses to images are calibrated relative to the Weber contrast of spatially-optimal spots of light. Since the three light-adaptation schemes actually produce the same answer (when expressed as equivalent contrast), for the remainder of this paper we will show only the behaviour of the centre-plus-surround adaptation scheme.

3.2. Equivalent contrast in natural scenes

The form of the equivalent-contrast distribution is almost independent of the adaptation scheme, but Fig. 4 shows that the form *does* depend to some extent upon

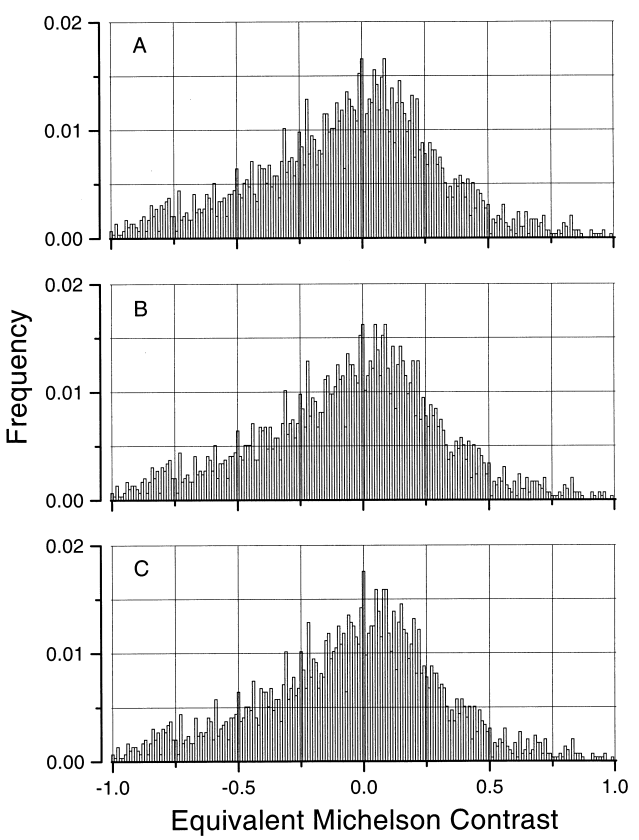

Fig. 3. The frequency distributions of the equivalent Michelson contrasts in the picture of the tree (Fig. 1C) are shown for the three light-adaptation schemes: the centre-only (A), the surround-only (B) and the centre-plus-surround (C). The outputs of the operator in Fig. 1 were transformed into equivalent Michelson contrasts for each light-adaptation scheme separately, using the appropriate contrast-output functions in Fig. 2 (see text).

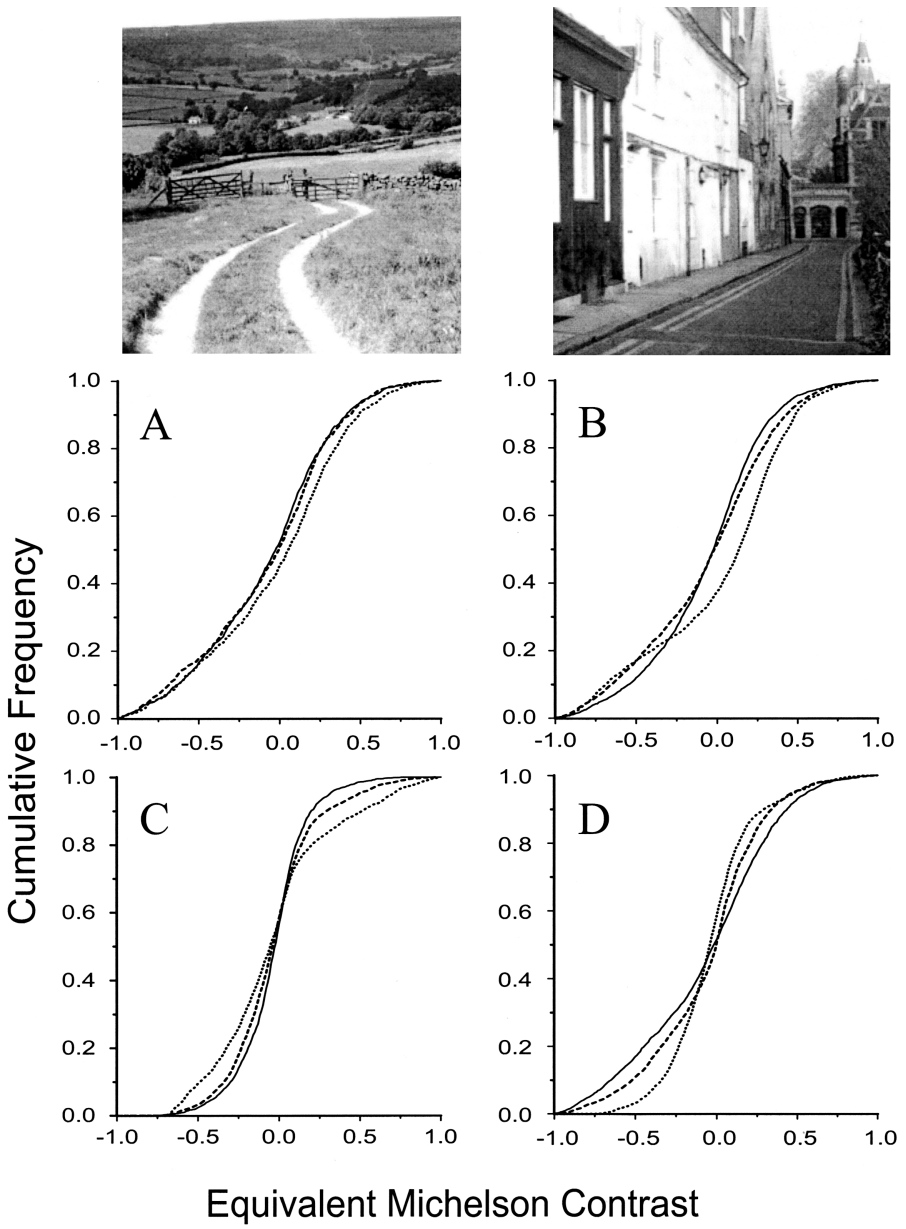

Fig. 4. Cumulative frequency distributions of the equivalent Michelson contrasts are shown for a variety of contrast operators, *all of which are subject to the centre-plus-surround light adaptation scheme*. (A) Equivalent Michelson contrasts in the picture of the tree (Fig. 1C) are shown for contrast operators all with a constant surround:centre ratio (r_s/r_c) of 4.0 but different centre radii (r_c) of 2.0 pixels (solid line), 3.0 pixels (dashed line) or 4.0 pixels (dotted line). (B) The effect of changing the surround:centre ratio (r_s/r_c) while keeping the centre radius constant at 2.0 pixels. The three operators had surround:centre ratios (r_s/r_c) of: 2.0, solid line; 4.0, dashed line; 8.0, dotted line. They were applied to the picture of the tree, as in (A). (C) The behaviour of the same three operators as in (B) when applied to a different natural scene, the countryside scene shown at top left. (D) The behaviour of a single contrast operator ($r_s = 2.0$ pixels; $r_s/r_c = 4.0$) to three different photographs: the tree (solid line), the countryside scene (dotted line) and a street scene shown at top right (dashed line).

other parameters of the model and upon the particular digitised photograph that is investigated. The distributions of equivalent contrast are shown as cumulative frequency distributions in order to facilitate comparison between different conditions.

Fig. 4A shows the distributions resulting from applying three different contrast operators to the digitised photograph of the tree branches (see Fig. 1C). The three operators differ in their receptive-field size while the surround:centre radius ratio is held constant at 4.0. The centre radius (r_c) in the three operators is 2.0, 3.0 or 4.0 pixels. For each operator, the output was calculated at 1000 locations in the photograph using the centre-plus-surround adaptation scheme; the outputs were transformed into equivalent contrasts using a contrast-output relation calculated with sinusoidal gratings

for each operator separately. The similarity of the three graphs in Fig. 4A shows that receptive-field size has very little effect on the estimates of the equivalent contrasts found in the photograph of the tree. This is consistent with the suggestion that natural scenes contain the same amount of power at all spatial scales (Burton & Moorhead, 1987; Field, 1987).

In Fig. 4B, the three contrast operators now differ in their surround:centre radius ratio (r_s/r_c of 2.0, 4.0 and 8.0), while the centre-size (r_c) is kept constant at 2.0 pixels. The distribution of equivalent contrast in the photograph of the tree branches *is* affected by surround:centre ratio; the contrast operator with the smallest ratio has the steepest curve (solid line), showing that it measures lower contrasts in the image than do the other two operators. This general finding is repeated when the same three contrast operators are applied to other digitised photographs. For instance, Fig. 4C shows the results of applying the same three operators to a different photograph, of a countryside scene (upper left in Fig. 4); the equivalent-contrast distributions for the three operators differ slightly from each other in much the same way as for Fig. 4B.

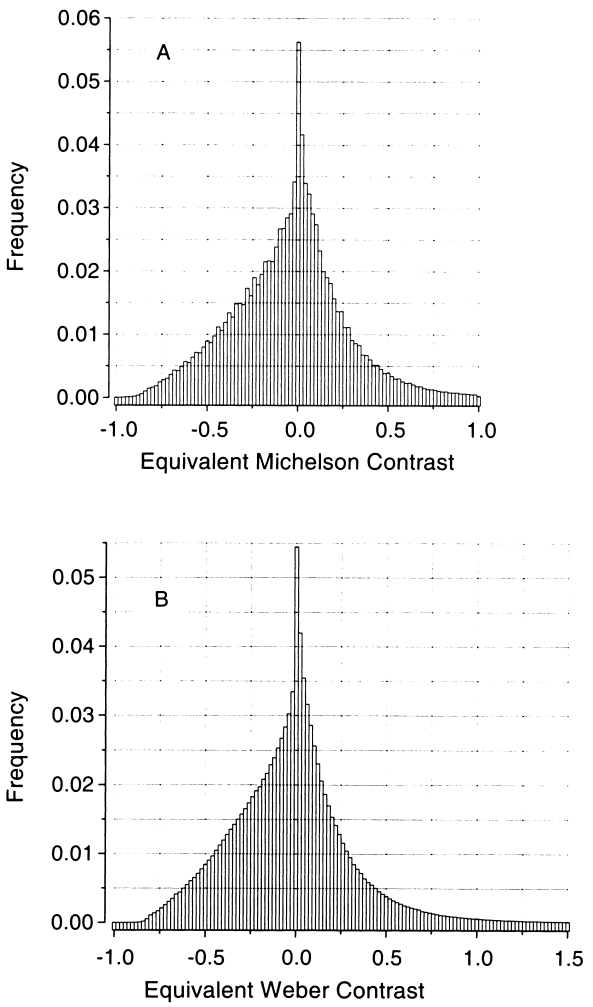

Fig. 5. (A) A summary of the distribution of the equivalent Michelson contrasts of the outputs of 24 different contrast operators, when applied at 1000 locations in each of 135 digitised photographs. Each operator was subjected to the centre-plus-surround light-adaptation scheme. The histogram shows the frequency as a proportion of 3.24 million simulated outputs. The mean equivalent contrast was 0.053 with a standard deviation of 0.300; we have not calculated kurtosis because this parameter would be greatly affected by the unplotted values with equivalent contrast above 1.0. (B) The same outputs to the 135 images were transformed into equivalent Weber contrast (the contrast of a spatially-optimal spot of light), and the distribution of the 3.24 million equivalent contrasts is plotted. The mean equivalent Weber was -0.028, with a standard deviation of 0.337. The normalised kurtosis of the full distribution (including the values greater than 1.5) was 7.58.

There are, however, noticeable differences between the distributions of Fig. 4B,C, indicating that different photographs contain different distributions of equivalent contrasts. This is illustrated further in Fig. 4D where one of the contrast operators (r_s/r_c of 4.0, r_c of 2.0) is applied to three different photographs (the tree branches, the countryside scene, and the street scene illustrated at top right in Fig. 4). It can be seen that the differences between the cumulative frequency distributions in Fig. 4D are somewhat larger than the differences found for the different surround:centre ratios in Fig. 4B,C.

In order to determine the range of contrasts that mammalian neurones will encounter in real world scenes we have used a variety of different contrast operators, representing the variety of spatial receptive-field characteristics of mammalian retinal ganglion cells and LGN neurones, and applied each operator to a large number of different natural scenes. The results in Fig. 4A–D demonstrate that, despite small differences, the overall sigmoidal forms of the cumulative frequency distributions for the different contrast operators or the different images are all *remarkably similar*. We have, therefore, decided to pool the results obtained with the different contrast operators as we describe in the next section.

3.3. The distribution of equivalent contrasts in natural images

Fig. 5A summarises the results of a large number of simulations, all using the centre-plus-surround adaptation scheme. A total of 135 digitised photographs were analysed with contrast operators with three different centre radii (r_c) at each of eight different surround:centre radius ratios. The output of each operator was calculated at 1000 locations in each photograph, resulting in more than 3 million estimates. The outputs of each of the 24 contrast operators were transformed into equivalent Michelson contrast using the appropriate contrast-output functions, measured with sinusoidal luminance gratings of optimal spatial frequency for of

each contrast operators separately. The figure shows the pooled transformed outputs of the 24 different operators that were applied to the 135 different photographs.

The histogram in Fig. 5A shows the frequency of occurrence of different equivalent Michelson contrasts in our ensemble of 135 natural images. The distribution has a distinct mode at zero contrast and it falls off almost exponentially with increasing positive and negative contrast values. The concave distribution is leptokurtic, implying that the majority of the contrasts in natural images as 'seen' by either ON-centre or OFF-centre mammalian neurones would be relatively low. This imply that it is very infrequent that a neurone finds the equivalent of its geometrically-simple optimal stimulus in a real world scene. In fact, about 90% of the occurrences have a Michelson contrast within the range ± 0.5. The distribution shows a slight asymmetry in the frequencies of positive and negative contrasts suggesting a small difference in the frequencies of bright and dark features in our photographs.

Although the Michelson contrast of a sinusoidal grating cannot exceed 1.0, it *is* possible for an ON-centre circularly-symmetric neurone to respond better to a bright spot of light within a natural image than it does to a grating of unit contrast, since the two-dimensional spot matches the centre-surround organisation of the receptive field better than does the one-dimensional grating. We have found that about 1% of the distribution lies at equivalent contrasts greater than 1.0, which we cannot plot.

Fig. 5B shows further simulations for the same set of contrast operators and photographs, but now the outputs of the operators have been transformed in a different way. Equivalent contrast has been calculated by comparison with the outputs of each operator to *spots of light of optimal radius* centred in the receptive field at a variety of Weber contrasts (Eq. (10)). Bright spots on a grey background have positive contrast, whereas dark spots on the same background have negative contrast. The distribution of equivalent Weber contrasts (Fig. 5B) is nearly identical to that of equivalent Michelson contrasts (Fig. 5A). Again, the equivalent Weber contrasts are generally rather low: only 10% of occurrences are outside the range ± 0.5. Eq. (10) shows that negative Weber contrasts cannot fall below -1.0, but there is no upper limit to the positive contrasts that could be achieved in theory: the spot of light could be many times brighter than the background. For instance, Hartveit and Heggelund (1992) stimulated LGN neurones with Weber contrasts as high as 7.0. However, our analysis suggests that only 0.5% of the equivalent Weber contrasts in natural images exceeds a contrast of 1.5.

4. Discussion

4.1. Suitable contrast operators for natural scenes

Since Kuffler's (1953) study of retinal ganglion cells in the cat, the receptive field organisation and the response properties of mammalian retinal ganglion cells and LGN neurones have been the subject of many studies. The stimuli used in the majority of these studies have been either spots of light or sinusoidal luminance gratings: geometrically-simple stimuli, designed to probe specific features of neuronal responses. Using these simple stimuli has made it possible to demonstrate, for instance, that the responses of mammalian retinal ganglion cells and of LGN neurones do not depend simply on the difference in the illumination (ΔI) of their antagonistic receptive-field regions but on stimulus contrast: $\Delta I/\bar{I}$ (Barlow, 1969a; Barlow & Levick, 1969a,b; Jacobs, 1969; Sakmann & Creutzfeldt, 1969; Shapley & Enroth-Cugell, 1984; Purpura et al., 1988; Troy & Enroth-Cugell, 1993).

Now that many of the response characteristics of these neurones have been established, we can examine to what degree their particular characteristics enable them to encode the information in real world scenes more efficiently (e.g. Srinivasan, Laughlin, & Dubs, 1982; Atick & Redlich, 1992; van Hateren, 1992; Levitt & Tadmor, 1995; Tadmor & Levitt, 1995; Dan, Atick, & Reid, 1996). In this paper we have calculated the range of contrasts that retinal ganglion cells and LGN neurones of the cat and monkey are likely to encounter in images of natural scenes. We have calculated the contrasts in real-world images using contrast operators that were based on the difference of Gaussians (DOG) model (Rodieck, 1965; Enroth-Cugell & Robson, 1966) since the DOG model has been used successfully to describe the receptive-fields and the responses to sinusoidal luminance gratings in many cat and monkey studies (e.g. Linsenmeier et al., 1982; Derrington & Lennie, 1982, 1984; Irvin et al., 1993; Donner & Hemilä, 1996; Croner & Kaplan, 1995; Benardete & Kaplan, 1997a).

It is important to recognise, however, that despite its success with sinusoidal luminance gratings, the conventional DOG model (Eq. (5)) cannot be used to predict the responses of neurones to real world images without a modification. The fundamental limitation of the DOG model is that it only describes the behaviour of neurones which are already light-adapted to a fixed light level; it does *not* acknowledge the process of light adaptation whereby the response sensitivity, or the gain, of neurones changes dynamically in accordance with the space-averaged mean illumination ($\bar{I}$). Since large variations of mean luminance from one location to another in images of real-world scenes are very common, we have had to modify the DOG model.

The required modification to the DOG model must ensure that the model produces outputs that depend on contrast ($\Delta I/\bar{I}$), rather than simply on the local luminance differences (ΔI). The simplest way to achieve this goal would be to normalise the output of the conventional DOG model by some measure of the space-averaged mean luminance. However, the problem we have faced when trying to implement this modification is the lack of any conclusive guidance from the physiological work on cat and monkey as to the exact size of this 'adaptation pool' (Rushton, 1965): the spatial extent over which the neurones evaluate the adapting signal. Some studies have reported that the adaptation pool has the same size as the receptive-field centre (Cleland & Enroth-Cugell, 1968; Enroth-Cugell et al., 1975; Shapley & Enroth-Cugell, 1984), while others have found that it may be as big as the surround (Kaplan & Shapley, 1989; Benardete & Kaplan, 1997b). It is not yet clear whether these disagreements reflect differences between cats and monkeys, or between X-cells and Y-cells, or between photopic and scotopic conditions.

In the absence of conclusive physiological guidance, we have chosen to examine three simple light adaptation schemes (Eqs. (6)–(8)): response gain was set by a value which is a weighted estimate of the mean luminance, calculated over either (i) the receptive-field centre alone, or (ii) the surround alone, or (iii) a combination of both. We have shown that, in detail, these three different light adaptation schemes predicted different neuronal responses to natural scenes. However, we have also shown that the predicted differences are exactly mirrored in the responses of the three adaptation schemes to gratings and spots of varying contrasts. Thus, when we expressed the calculated responses of our model neurones to the images as the *equivalent contrasts* of gratings or spots of light, the distributions of equivalent contrasts predicted by the different light adaptation schemes became virtually indistinguishable (Fig. 3).

We have not implemented more complex models in which the centre and surround components of the receptive field can adapt separately before the stage of spatial opponency (Cleland & Enroth-Cugell, 1968; Cleland & Freeman, 1988; Dahari & Spitzer, 1996; Shah & Levine, 1996; Wilson, 1997). Such models may be needed to account for the way in which response dynamics are affected by the adaptation level, but they do not seem necessary to our understanding of the steady-state situation as modelled in this paper. We consider only the steady-state condition since adaptation at photopic levels will occur quite rapidly compared to inter-saccadic intervales, so long as the mean luminance changes by no more than two log units (cf. Enroth-Cugell & Shapley, 1973). Nor have we tried to model the possibility that the adaptation pool may be smaller than the receptive field centre, as has been reported in cat Y-cells (Cleland & Freeman, 1988). A discussion of photoreceptor light adaptation and the possible contribution of retinal inter-neurones to the process of light adaptation can be found in Hood (1998).

An interesting challenge would be to relate our finding for retinal ganglion cells and LGN neurones to those of Peli (1990, 1997) who introduced a similar computational scheme to the one we have used here in order to model the perceived contrasts of natural images and of Gabor patches. It would also be interesting to extend our model to include the effects of *contrast-gain control*, a process whereby the neurone's response gain is altered by the contrast (as well as the luminance) of the stimuli that fall within and around the classical receptive-field (Shapley & Victor, 1978; Valberg et al., 1985; Smirnakis, Berry, Warland, Bialek, & Meister, 1997).

4.2. Optimised representation of contrasts in natural scenes

Here, we have used relatively simple models of the receptive-fields of mammalian neurones to determine the distributions of equivalent Michelson and Weber contrasts in a large number of natural scenes (Fig. 5). We have found that these distributions exhibits two distinct features. First, the most frequently encountered contrast value is zero contrast. Secondly, these unimodal distributions are very concave (or leptokurtic) and fall off roughly as an exponential function of increasing and decreasing contrasts. Thus, our computational modelling predicts that the great majority of the contrasts that retinal ganglion cells and LGN neurones encounter in natural scenes are low, whereas high contrasts are very infrequent. This prediction has been confirmed recently in single-cell electrophysiological measurements of the responses of macaque LGN neurones when viewing images of natural scenes (Levitt & Tadmor, 1995; Tadmor & Levitt, 1995): the response distributions of single cells show that the most frequent response level is, indeed, zero extra spikes/s above the spontaneous level and that, very infrequently, the neurones produce high responses.

This particular form of concave (or leptokurtic) distribution, as in Fig. 5, is consistent with the suggestion that the representation of visual information in the whole population of neurones is sparse (e.g. Barlow, 1969b, 1989; Field, 1987; Olshausen & Field, 1996); a representation which efficiently exploits the redundancies in natural scenes. It should be noted, however, that although our results are consistent with sparse coding models, the leptokurtic form of the distributions is not a direct proof for a sparse representation since kurtosis may arise for other reasons (Baddeley, 1996).

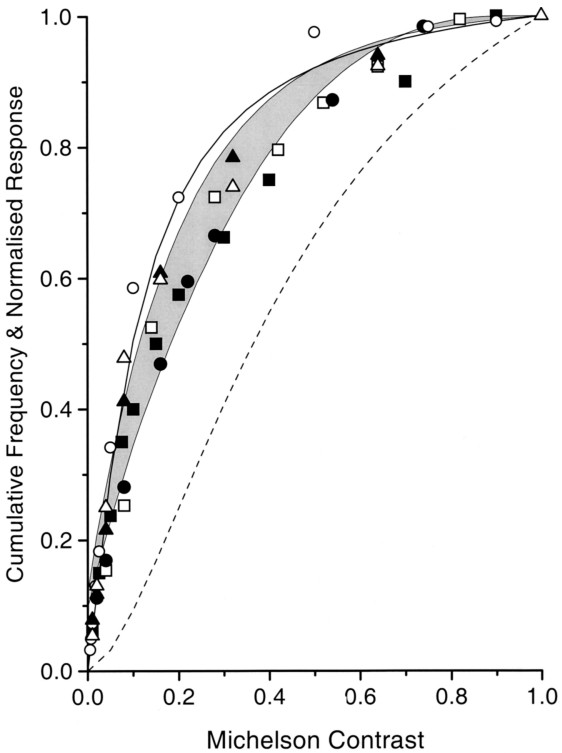

Fig. 6. A comparison between published responses of real neurones to sinusoidal luminance gratings of different Michelson contrasts and the cumulative frequency of the equivalent Michelson contrast calculated from natural scenes. The responses of real neurones were normalised to a value of 1.0 at a Michelson contrast of 1.0, or to the corresponding value of the cumulative contrast frequency whenever the published data did not extend to 1.0 contrast. The shaded area shows the upper and lower values of the integrals of the frequency distribution in Fig. 5A: the upper curve is the cumulative frequency calculated from a contrast of zero upwards and the lower curve is for the negative contrasts. The line graphs show the contrast-response functions for macaque LGN M cells (solid line) and P cells (dashed line) from the equations that Sclar et al. (1990) fitted to a large number of cells. The individual symbols show data for cat X (filled symbols) and Y (open symbols) cells, replotted from several sources: (△ ▲) nonlagged, LGN neurones from Saul and Humphrey (1990, Fig. 13); (○ ●) retinal ganglion cells from Troy and Enroth-Cugell (1993, Figs. 2 & 3); (□ ■) retinal ganglion cells from Rowe and Cox (1993, Figs. 9 & 10).

Laughlin (1981) suggested that, for maximal efficiency, the limited dynamic response range of individual visual neurones should match the distribution of contrasts in the natural environment. Indeed, in the fly, contrast response functions matched the cumulative frequency distribution of contrasts which fly neurones find in the natural environment (Laughlin, 1981). Since our contrast analysis has determined the frequency distributions of contrasts that mammalian neurones find in natural scenes, we can now examine whether Laughlin's conclusions for the fly also apply for neurones in the retina and LGN of cat and monkey.

Fig. 6 shows the cumulative frequency of equivalent Michelson contrasts in natural scenes, calculated from the distribution in Fig. 5A, along with several published measurements of contrast-response functions of neurones in retina and LGN of cat and monkey. The shaded area in Fig. 6 shows the cumulative frequency of equivalent Michelson contrasts. The area is bounded above by the integral of positive contrasts (from zero contrast upwards) and, below, by the integral of the negative contrasts; the contrasts that will be seen by OFF-centre neurones. The line graphs show the forms of the contrast-response functions for macaque LGN M-cells (solid line) and P-cells (dashed line) from the equations that Sclar, Maunsell, and Lennie (1990) fitted to a large number of cells. The equations for macaque M- and P-retinal ganglion cells reported by Kaplan, Lee, and Shapley (1990) were virtually identical to the LGN graphs and are, therefore, not shown. The individual symbols show data for cat X (filled symbols) and Y (open symbols) cells, replotted from several sources, specified in the figure legend.

It can be seen that the form of the contrast-response functions of cat X- and Y-cells and of the monkey's M-cells match almost exactly the contrasts we have predicted that they would 'see' in the natural environment, in agreement with Laughlin's (1981, 1983) conclusion for the fly. However, it is quite clear that the responses of the macaque's P-cells (dashed line) are *not* a close match to our estimates of the contrasts in the natural environment. This is not entirely surprising since the receptive-fields of P-cells, unlike M-cells or cat X- and Y-cells, are colour-opponent, a property which we have not included in our modelling of their responses to *monochrome* natural images. For a detailed discussion of the chromatic selectivity of P-cells and its possible consequences on the contrast responses of P-cells see Kaplan et al. (1990).

Acknowledgements

We thank H.B. Barlow, S.B. Laughlin and J.D. Mollon for helpful comments and discussions. The work was supported by a Wellcome Trust Research Fellowship (# 036403 & # 047064) to YT.

References

Atick, J. J., & Redlich, A. N. (1992). What does the retina know about natural scenes? *Neural Computation*, *4*, 196–210.

Baddeley, R. (1996). Searching for filters with interesting output distributions — an uninteresting direction to explore. *Network Computation in Neural Systems*, *7*, 409–421.

Barlow, H. B. (1969a). Pattern recognition and the responses of sensory neurons. *Annals Of The New York Academy Of Sciences*, *156*, 872–881.

Barlow, H. B. (1969b). Trigger features, adaptation and economy of impulses. In K. N. Leibovic, *Information processing in the nervous system* (pp. 209–226). New York: Springer-Verlag.

Barlow, H. B., & Levick, W. R. (1969a). Three factors limiting the reliable detection of light by retinal ganglion cells of the cat. *Journal of Physiology*, *200*, 1–24.

Barlow, H. B., & Levick, W. R. (1969b). Coding of light intensity by the cat retina. *Rendiconti della Scoula Int. di Fisica "Enrico Fermi", XLIII corso* (pp. 385–396). Academic Press.

Barlow, H. B. (1989). Unsupervised learning. *Neural Computation*, *1*, 295–311.

Benardete, E. A., & Kaplan, E. (1997a). The receptive field of the primate P retinal ganglion cell, I: linear dynamics. *Visual Neuroscience*, *14*, 169–185.

Benardete, E. A., & Kaplan, E. (1997b). The receptive field of the primate P retinal ganglion cell, II: nonlinear dynamics. *Visual Neuroscience*, *14*, 187–205.

Burton, G. J., & Moorhead, I. R. (1987). Colour and spatial structure in natural scenes. *Applied Optics*, *26*, 157–170.

Cleland, B. G., & Enroth-Cugell, C. (1968). Quantitative aspects of sensitivity and summation in the cat retina. *Journal of Physiology*, *198*, 17–38.

Cleland, B. G., & Freeman, A. W. (1988). Visual-adaptation is highly localised in the cat's retina. *Journal of Physiology*, *404*, 591–611.

Croner, L. J., & Kaplan, E. (1995). Receptive fields of P-ganglion and M-ganglion cells across the primate retina. *Vision Research*, *35*, 7–24.

Dahari, R., & Spitzer, H. (1996). Spatiotemporal adaptation model for retinal ganglion cells. *Journal of the Optical Society of America*, *A*, *13*, 419–435.

Dan, Y., Atick, J. J., & Reid, R. C. (1996). Efficient coding of natural scenes in the lateral geniculate nucleus — experimental test of a computational theory. *Journal of Neuroscience*, *16*, 3351–3362.

Derrington, A. M., & Lennie, P. (1982). The influence of temporal frequency and adaptation level on receptive field organisation of retinal ganglion cells in cat. *Journal of Physiology*, *333*, 343–366.

Derrington, A. M., & Lennie, P. (1984). Spatial and temporal contrast sensitivities of neurones in lateral geniculate nucleus of macaque. *Journal of Physiology*, *357*, 219–240.

Donner, K., & Hemilä, S. (1996). Modelling the spatio-temporal modulation response of ganglion cells with difference-of-Gaussians receptive fields: relation to photoreceptor response kinetics. *Visual Neuroscience*, *13*, 173–186.

Enroth-Cugell, C., & Shapley, R. M. (1973). Adaptation and dynamics of cat retinal ganglion cells. *Journal of Physiology*, *233*, 271–309.

Enroth-Cugell, C., Lennie, P., & Shapley, R. M. (1975). Surround contribution to light adaptation in cat retinal ganglion cells. *Journal of Physiology*, *247*, 579–588.

Enroth-Cugell, C., & Robson, J. G. (1966). The contrast sensitivity of retinal ganglion cells of the cat. *Journal of Physiology*, *187*, 517552.

Field, D. J. (1987). Relations between the statistics of natural images and the response properties of cortical cells. *Journal of the Optical Society of America*, *A*, *4*, 2379–2394.

Hartveit, E., & Heggelund, P. (1992). The effect of contrast on the visual response of lagged and nonlagged cells in the cat lateral geniculate-nucleus. *Visual Neuroscience*, *9*, 515–525.

Hood, D. C. (1998). Lower-level visual processing and models of light adaptation. *Annual Review of Psychology*, *49*, 503–535.

Irvin, G. E., Casagrande, V. A., & Norton, T. T. (1993). Center surround relationships of magnocellular, parvocellular, and koniocellular relay cells in primate lateral geniculate nucleus. *Visual Neuroscience*, *10*, 363–373.

Jacobs, G. H. (1969). Effects of adaptation on the lateral geniculate response to light increment and decrement. *Journal of the Optical Society of America*, *55*, 1535–1540.

Kaplan, E., & Shapley, R. M. (1989). Illumination of the receptive field surround controls the contrast gain of macaque P retinal ganglion cells. *Society of Neuroscience Abstracts*, *15*, 174.

Kaplan, E., Lee, B. B., & Shapley, R. M. (1990). New views of primate retinal function. *Progress in Retinal Research*, *9*, 273–336.

Kuffler, S. W. (1953). Discharge patterns and functional organization of mammalian retina. *Journal of Neurophysiology*, *16*, 37–68.

Laughlin, S. B. (1981). A simple coding procedure enhances a neuron's information capacity. *Zeitschrift für Naturforschung Section C Biosciences*, *36*, 910–912.

Laughlin, S. B. (1983). Matching coding to scenes to enhance efficiency. In O. J. Braddick, & A. C. Sleigh, *Physical and biological processing of images* (pp. 42–52). Berlin: Springer-Verlag.

Levitt, J. B., & Tadmor, Y. (1995). Response of primate LGN neurones to natural images. *Society for Neuroscience Abstracts*, *21*, 657.

Linsenmeier, R. A., Frishman, L. J., Jakiela, H. G., & Enroth-Cugell, C. (1982). Receptive-field properties of X-cells and Y-cells in the cat retina derived from contrast sensitivity measurements. *Vision Research*, *22*, 1173–1183.

Martin, G. R. (1983). Schematic eye models in vertebrates. *Progress in Sensory Physiology*, *4*, 44–81.

Peli, E. (1990). Contrast in complex images. *Journal of the Optical Society of America*, *A*, *7*, 2032–2040.

Peli, E. (1997). In search of a contrast metric: matching the perceived contrast of Gabor patches at different phases and bandwidths. *Vision Research*, *37*, 3217–3224.

Purpura, K., Kaplan, E., & Shapley, R. M. (1988). Background light and the contrast gain of primate P and M retinal ganglion cells. *Proceedings of the National Academy of Sciences*, *85*, 4534–4537.

Olshausen, B. A., & Field, D. J. (1996). Emergence of simple-cell receptive field properties by learning a sparse code for natural images. *Nature*, *381*, 607–609.

Rodieck, R. (1965). Quantitative analysis of cat retinal ganglion cell response to visual stimuli. *Vision Research*, *5*, 583–601.

Rowe, H. M., & Cox, J. F. (1993). Spatial receptive-field structure of cat retinal W-cells. *Visual Neuroscience*, *10*, 765–779.

Rushton, W. A. H. (1965). Light adaptation. *Proceedings of the Royal Society*, *B*, *162*, 20–46.

Sakmann, B., & Creutzfeldt, O. D. (1969). Scotopic and mesopic light adaptation in the cat's retina. *Pflügers Archives*, *313*, 168–185.

Saul, A. B., & Humphrey, A. L. (1990). Spatial and temporal response properties of lagged and nonlagged cells in the cat lateral geniculate nucleus. *Journal of Neurophysiology*, *64*, 206–224.

Sclar, G., Maunsell, J. H. R., & Lennie, P. (1990). Coding of image-contrast in central visual pathways of the macaque monkey. *Vision Research*, *30*, 1–10.

Shah, S., & Levine, M. D. (1996). Visual information processing in primate cone pathways – part I: a model. *IEEE Trans. Syst. Man Cybern.*, *26*, 259–274.

Shapley, R. M., & Enroth-Cugell, C. (1984). Visual adaptation and retinal gain controls. *Progress in Retinal Research*, *3*, 263–346.

Shapley, R. M., & Victor, J. D. (1978). The effect of contrast on the transfer properties of cat retinal ganglion cells. *Journal of Physiology*, *285*, 275–298.

Smirnakis, S. M., Berry, M. J., Warland, D. K., Bialek, W., & Meister, M. (1997). Adaptation of retinal processing to image contrast and spatial scale. *Nature*, *386*, 69–73.

Srinivasan, M. V., Laughlin, S. B., & Dubs, A. (1982). Predictive coding: a fresh view of inhibition in the retina. *Proceedings of the Royal Society of London*, *B*, *216*, 427–459.

Tadmor, Y., & Levitt, J. B. (1995). What do primate LGN neurones see in natural images? *Perception*, *24*, 8A.

Tadmor, Y., & Tolhurst, D. J. (1994). Discrimination of changes in the second-order statistics of natural and synthetic images. *Vision Research*, *34*, 541–554.

Tadmor, Y., & Tolhurst, D. J. (1995). The contrasts in natural scenes and their representation by mammalian retinal and geniculate neurones. In M. Burrows, T. Matheson, P. L. Newland, & H. Schuppe, *Nervous systems and behaviour. Proceedings of the 4th*

International Congress of Neuroethology. Stuttgart: Georg Thieme Verlag.

Tolhurst, D. J., & Tadmor, Y. (1997). Band-limited contrast in natural images explains the detectability of changes in the amplitude spectra. *Vision Research*, *37*, 3203–3215.

Tolhurst, D. J., Tadmor, Y., & Tang Chao (1992). The amplitude spectra of natural images. *Ophthalmic and Physiological Optics*, *12*, 229–232.

Troy, J. B., & Enroth-Cugell, C. (1993). X-ganglion and Y-ganglion cells inform the cat's brain about contrast in the retinal image. *Experimental Brain Research*, *93*, 383–390.

Valberg, A., Lee, B. B., & Tigwell, D. A. (1985). A simultaneous contrast effect of steady remote surrounds on responses of cells in the macaque lateral geniculate nucleus. *Experimental Brain Research*, *58*, 604–608.

van Hateren, J. H. (1992). Theoretical predictions of spatiotemporal receptive fields of fly LMCs, and experimental validation. *Journal of Comparative Physiology*, *A*, *171*, 157–170.

von Helmholtz, H. (1924). In J. P. C Southall, *Physiological optics*, vol. 2. New York: Dover Publications.

Wilson, H. R. (1997). A neural model of foveal light adaptation and afterimage formation. *Visual Neuroscience*, *14*, 403–423.

Wyszecki, G., & Stiles, W. S. (1982). *Colour science*. New York: Wiley.